TD Radiation Properties of Array Antennas Composed of Pulsed Electric-Current Excited Elements

Lager, Ion E.; de Hoop, Adrianus T.

DOI
10.1109/LAWP.2014.2377071

Publication date
2015

Document Version
Accepted author manuscript

Published in
IEEE Antennas and Wireless Propagation Letters

TD Radiation Properties of Array Antennas Composed of Pulsed Electric-Current Excited Elements

Ioan E. Lager, *Senior Member, IEEE*, and Adrianus T. de Hoop, *Life Member, IEEE*

***Abstract*—A full time-domain analysis is presented of the radiation properties of array antennas composed of identical, mutually translationally shifted, pulsed electric-current excited elements. An expression is derived for the radiated field in the far-field region, the parameters in which provide the basis for studying the pulsed-field beam-shaping and beam-steering properties of the array. Mutual coupling is neglected. Computational results illustrate the influence of the different parameters.**

***Index Terms*—Antenna arrays, antenna radiation patterns, beam steering, time-domain analysis.**

I. Introduction

ULTRAWIDEBAND (UWB) systems have pervaded the wireless technology, with ultra-fast digital transfer and high-resolution (medical) imaging as the fastest growing areas of applicability. A key enabler in designing any UWB system is the characterization of antenna (arrays) over very large bandwidths. Such tasks are habitually carried out by resorting to the instruments of the frequency-domain (FD) theory of (array) antennas, with standard textbooks (such as [1]) fully covering the relevant features and performance metrics. However, the FD analyses and metrics are ill-adapted for UWB radiation studies [2].

The *pulsed electromagnetic* (EM) field radiation is adequately studied via time-domain (TD) instruments. Such analyses are less frequent in the literature, with [3]–[8] discussing the theoretical background, [2] the beamforming, and [9]–[11] the applicable performance metrics. Here, we note that, in an attempt to establish parallels with the well-known FD grating lobes, [10] employed trains of pulses as excitation. Nonetheless, in digital communications, (long) trains of pulses limit the achievable data rate, with coded single-pulse excitation offering superior performance. Then, we henceforth restrict the term "pulsed EM field" to single-pulse excitation.

This type of radiation was examined analytically for thin wire radiators in [12] and for elementary radiators (dipoles and loops) in [13, Sec. 26.9 and 26.10] and [14]. Furthermore, [5] and [7] analyzed array antennas operated in this regime.

Manuscript received October 15, 2014; revised November 16, 2014; accepted November 19, 2014. Date of publication December 04, 2014; date of current version March 02, 2015.

The authors are with the Faculty of Electrical Engineering, Mathematics and Computer Science, Delft University of Technology, 2628 CD Delft, The Netherlands (e-mail: i.e.lager@tudelft.nl; a.t.dehoop@tudelft.nl).

Color versions of one or more of the figures in this letter are available online at http://ieeexplore.ieee.org.

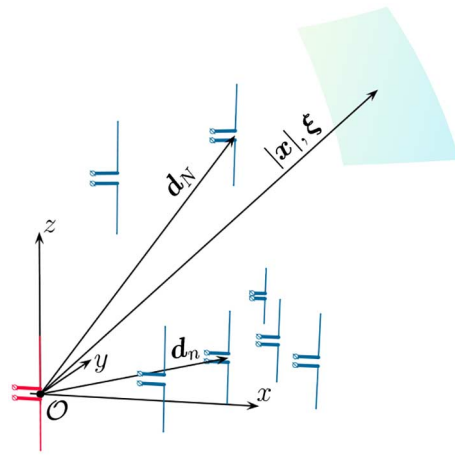

Fig. 1. Antenna array composed of identical, mutually translationally shifted elements.

The pulsed EM field radiation properties of an antenna array composed of electric current carrying elements are studied analytically in this letter via a full TD methodology. The number of elements is arbitrary but finite. The elements are excited by pulsed electric currents fed into them via a one-port Kirchhoff circuit. Our analysis can serve a purpose in the design of UWB and/or pulsed EM field sparse arrays.

II. Description of the Configuration

The antenna consists of $N+1, N = 0, 1, 2\ldots$, identical, mutually translationally shifted, pulsed electric-current excited elements (Fig. 1). Position in the configuration is specified by the position vector $\boldsymbol{x} \in \mathbb{R}^3$. The time coordinate is $t \in \mathbb{R}$.

Let $\mathcal{D}_0$ denote the spatial support of the reference element, and let $\chi_0(\boldsymbol{x})$ be its characteristic set, i.e., $\chi_0(\boldsymbol{x}) = \{0, 1/2, 1\}$ for $\boldsymbol{x} \in \{\mathcal{D}_0, \partial\mathcal{D}_0, \mathcal{D}_0^\infty\}$, where $\partial\mathcal{D}_0$ is the piecewise smooth boundary of $\mathcal{D}_0$ and $\mathcal{D}_0^\infty$ is the (unbounded) complement of $\mathcal{D}_0 \cup \partial\mathcal{D}_0$ in $\mathbb{R}^3$. The spatial support $\mathcal{D}_n$ of the $\boldsymbol{d}_n$ with respect to $\mathcal{D}_0$ translationally shifted element has the characteristic set $\chi_n(\boldsymbol{x}) = \chi_0(\boldsymbol{x} + \boldsymbol{d}_n)$. The support of the entire array is $\mathcal{D} = \bigcup_{n=0}^{N} \mathcal{D}_n$.

The array elements carry electric currents with volume density $\boldsymbol{J}(\boldsymbol{x}, t)$. The array radiates into free space with electric permittivity ε_0, magnetic permeability μ_0, and corresponding

wave speed $c_0 = (\varepsilon_0\mu_0)^{-1/2}$. Each element is accessible via a one-port Kirchhoff circuit. The volume densities of electric current in $\mathcal{D}_n$ are $\boldsymbol{J}_n^\delta(\boldsymbol{x},t)$ in case its Kirchhoff circuit port is excited with a Dirac delta pulse and, correspondingly

$$\boldsymbol{J}_n(\boldsymbol{x},t) = I_n^G(t) \overset{(\boldsymbol{t})}{*} \boldsymbol{J}_n^\delta(\boldsymbol{x},t) \tag{1}$$

in case its Kirchhoff circuit port is excited with the electric current $I_n^G(t)$, with $\overset{(\boldsymbol{t})}{*}$ denoting time convolution. Neglecting mutual coupling, we have

$$\boldsymbol{J}_n^\delta(\boldsymbol{x},t) = \boldsymbol{J}_0^\delta(\boldsymbol{x}+\boldsymbol{d}_n,t), \qquad \text{for } n = 1,\ldots,N. \tag{2}$$

III. Radiated Field

The radiated field is expressible in terms of the electric-current potential $\boldsymbol{A}(\boldsymbol{x},\boldsymbol{t})$ that satisfies the vector wave equation

$$(\boldsymbol{\nabla}\cdot\boldsymbol{\nabla})\boldsymbol{A} - c_0^{-2}\partial_t^2\boldsymbol{A} = -\sum_{n=0}^{N}\boldsymbol{J}_n(\boldsymbol{x},t)\chi_n(\boldsymbol{x},t). \tag{3}$$

With

$$G(\boldsymbol{x},t) = \frac{\delta(t-|\boldsymbol{x}|/c_0)}{4\pi|\boldsymbol{x}|} \qquad \text{for } \boldsymbol{x}\neq\boldsymbol{0} \tag{4}$$

as the Green's function of the scalar wave equation

$$(\boldsymbol{\nabla}\cdot\boldsymbol{\nabla})G - c_0^{-2}\partial_t^2 G = -\delta(\boldsymbol{x},t) \tag{5}$$

it follows that

$$\boldsymbol{A}(\boldsymbol{x},t) = \sum_{n=0}^{N}\boldsymbol{A}_n(\boldsymbol{x},t) = \sum_{n=0}^{N} G(\boldsymbol{x},t) \overset{(\boldsymbol{x})}{*} \overset{(t)}{*} \boldsymbol{J}_n(\boldsymbol{x},t) \qquad \text{for } \boldsymbol{x}\in\mathbb{R}^3 \tag{6}$$

in which $\overset{(\boldsymbol{x})}{*}$ denotes spatial convolution (extended over $\mathcal{D}$). From Maxwell's equations, the corresponding electric and magnetic field strengths are [13, Eqs. (26.3-1) and (26.3-2)]

$$\boldsymbol{E} = -\mu_0\partial_t\boldsymbol{A} + \epsilon_0^{-1}\mathbf{I}_t\boldsymbol{\nabla}(\boldsymbol{\nabla}\cdot\boldsymbol{A}) \tag{7}$$

$$\boldsymbol{H} = \boldsymbol{\nabla}\times\boldsymbol{A} \tag{8}$$

where $\mathbf{I}_t$ denotes time integration $\int_{\tau=-\infty}^{t} f(\tau)\mathrm{d}\tau$.

IV. TD Far-Field Radiation Characteristics

Let the TD far-field expression

$$\{\boldsymbol{A},\boldsymbol{E},\boldsymbol{H}\}(\boldsymbol{x},t) = \frac{\{\boldsymbol{A}^\infty,\boldsymbol{E}^\infty,\boldsymbol{H}^\infty\}(\boldsymbol{\xi},t-|\boldsymbol{x}|c_0^{-1})}{4\pi|\boldsymbol{x}|}\left[1+O(|\boldsymbol{x}|^{-1})\right] \qquad \text{as } |\boldsymbol{x}|\to\infty \tag{9}$$

with $\mathcal{O}$ as the reference center and $\boldsymbol{\xi} = \boldsymbol{x}/|\boldsymbol{x}|$ as the unit vector in the direction of observation. The far-field radiation characteristics $\{\boldsymbol{A}^\infty,\boldsymbol{E}^\infty,\boldsymbol{H}^\infty\}(\boldsymbol{\xi},t)$ are then interrelated by [13, Eqs. (26.12-6) and (26.12-7)]

$$\boldsymbol{E}^\infty = -\mu_0[\partial_t\boldsymbol{A}^\infty - \boldsymbol{\xi}(\boldsymbol{\xi}\cdot\partial_t\boldsymbol{A}^\infty)] \tag{10}$$

$$\boldsymbol{H}^\infty = -c_0^{-1}\boldsymbol{\xi}\times\partial_t\boldsymbol{A}^\infty. \tag{11}$$

V. Beam Shaping and Beam Steering of the Array

For a given positioning of the elements of the array, standard practice for its beam shaping and beam steering is to select a reference pulse $I_0^{\mathrm{G}}(t)$ for exciting $\mathcal{D}_0$ and taking $\{I_n^{\mathrm{G}}(t); n = 1,2,3,\ldots,N\}$ to be time-shifted versions of it $I_n^{\mathrm{G}}(t) = I_0^{\mathrm{G}}(t-T_n)$, with T_n the relevant time delays. With (1) and (2), then

$$\boldsymbol{A}^\infty = \sum_{n=0}^{N}\boldsymbol{A}_n^\infty = \sum_{n=0}^{N}\left\{I_0^{\mathrm{G}}(t-T_n) \overset{(\boldsymbol{t})}{*} \int_{\mathcal{D}_n}\boldsymbol{J}_0^\delta[\boldsymbol{x}',t+c_0^{-1}\boldsymbol{\xi}\cdot(\boldsymbol{x}'+\boldsymbol{d}_n)]\mathrm{d}V(\boldsymbol{x}')\right\}. \tag{12}$$

By rewriting this time convolution, it follows that constructive interference of the element contributions occurs if

$$T_n = c_0^{-1}\boldsymbol{\xi}_{\mathrm{st}}\cdot\boldsymbol{d}_n, \qquad \text{for } n = 1,2,3,\ldots,N. \tag{13}$$

The resulting $\boldsymbol{\xi}_{\mathrm{st}}$ specifies the direction of the main beam ("direction of steering").

VI. Area Density of Radiated Energy

The energy W^{rad} radiated by the array is expressed as

$$W^{\mathrm{rad}} = \int_{\boldsymbol{\xi}\cdot\boldsymbol{\xi}=1}\boldsymbol{\Phi}^{\mathrm{rad}}(\boldsymbol{\xi})\cdot\boldsymbol{\xi}\mathrm{d}\Omega \tag{14}$$

in which $\boldsymbol{\Phi}^{\mathrm{rad}}(\boldsymbol{\xi})$ is the area density of radiated energy in the direction $\boldsymbol{\xi}$. Since the embedding medium is lossless, $\boldsymbol{\Phi}^{\mathrm{rad}}(\boldsymbol{\xi})$ can be expressed in terms of the far-field quantities introduced in Section III. The EM energy balance (the Poynting theorem) and (9)–(14) lead to

$$\boldsymbol{\Phi}^{\mathrm{rad}}(\boldsymbol{\xi}) = \frac{1}{16\pi^2}\int_{t\in\mathbb{R}}(\boldsymbol{E}^\infty\times\boldsymbol{H}^\infty)\,\mathrm{d}t. \tag{15}$$

Using (9)–(11), it follows that

$$\boldsymbol{\Phi}^{\mathrm{rad}}(\boldsymbol{\xi}) = \frac{Z_0}{16\pi^2 c_0^2}\,\boldsymbol{\xi}\int_{t\in\mathbb{R}}[\partial_t\,(\boldsymbol{\xi}\times\boldsymbol{A}^\infty)\cdot\partial_t\,(\boldsymbol{\xi}\times\boldsymbol{A}^\infty)]\mathrm{d}t \tag{16}$$

with $Z_0 = (\mu_/\epsilon_0)^{1/2}$ denoting the free-space electromagnetic wave impedance.

VII. Numerical Illustrations

Sections IV–VI provide the full TD expressions of the far field radiated by an array antenna in its dependence on the parameters involved (positioning of the elements, pulse shapes, and amplitudes of a sequence of feeding electric currents). The purpose of these numerical illustrations is to elucidate the role of these parameters on beam shaping [the beam steering following by adjusting the time delays T_n in (12)]. The examples will also highlight the constructive and destructive interference of the fields radiated by the array's elements.

In our analysis, we use polar diagrams of the quantity

$$D_{\mathrm{dB}}(\boldsymbol{\xi}) = 10\log_{10}\left[\boldsymbol{\Phi}^{\mathrm{rad}}(\boldsymbol{\xi})\cdot\boldsymbol{\xi}/4\pi W^{\mathrm{rad}}\right] \tag{17}$$

namely the area density of the radiated energy normalized with respect to the one corresponding to an isotropic radiator.

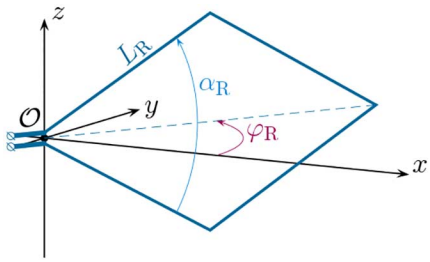

Fig. 2. Rhombic antenna element. Its geometric parameters are the opening angle α_R and the side length L_R.

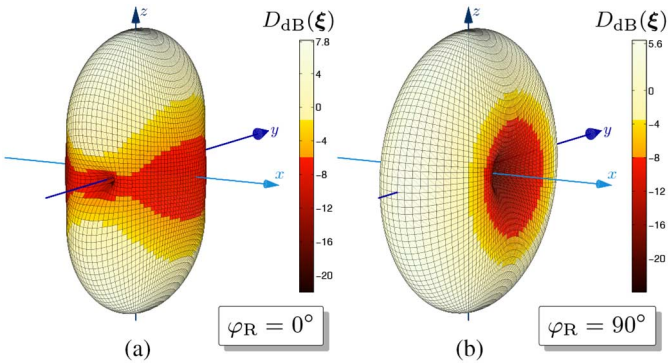

Fig. 3. $D_{dB}(\boldsymbol{\xi})$ pattern for a uniform, linear array consisting of eight rhombic antennas; $4\sqrt{2}L_R$ interelement spacing; broadside beam steering. The elements in the array are rotated at (a) $\varphi_R = 0°$ and (b) $\varphi_R = 90°$.

The shape of the electric current pulses is taken to be the one of the normalized power-exponential (PE) pulses [15]

$$I(t) = I_{max}(t/t_r)^{\nu} \exp\left[-\nu\left(t/t_r - 1\right)\right] H(t) \qquad (18)$$

where I_{max} is the pulse amplitude, $t_r > 0$ the pulse rise time, $\nu > 0$ the pulse rising power, and $H(\cdot)$ the Heaviside unit step function. For the majority of practical applications, ν can be taken as integer, a choice that is henceforth enforced. In [15], it was shown that such pulses can be generated by means of simple passive circuitry. Note that a sequence of such unipolar pulses cannot lead to destructive interference unless amplitudes of alternating signs are used. This implies that if nulls are desired, somewhere a change in sign has to be impressed.

Henceforth, we focus on linear arrays with elements located along the $\mathcal{O}x$-axis. The elementary radiators are taken to consist of electric current carrying thin wire segments, the far field radiated by these segments being discussed in the Appendix. Such a typical radiator is the rhombic wire antenna [16] (see Fig. 2). In all experiments, $\alpha_R = 90°$ and $L_R = c_0 t_w/20$, with t_w being the pulse time width of the feeding electric current. For this type of radiator, the $D_{dB}(\boldsymbol{\xi})$ has the "doughnut" shape that is characteristic for dipoles, with the nulls in the direction perpendicular to the rhombus's plane (the relevant plots are omitted for brevity).

A. Uniform Array Analysis

First, we study the behavior of broadside, linear, uniform arrays consisting of eight rhombic antennas. The $D_{dB}(\boldsymbol{\xi})$ is plotted in Figs. 3 and 4 for interelement spacings of $4\sqrt{2}L_R$ and $160\sqrt{2}L_R$, respectively. The plots clearly illustrate the beamwidth decreases with increasing interelement spacing and,

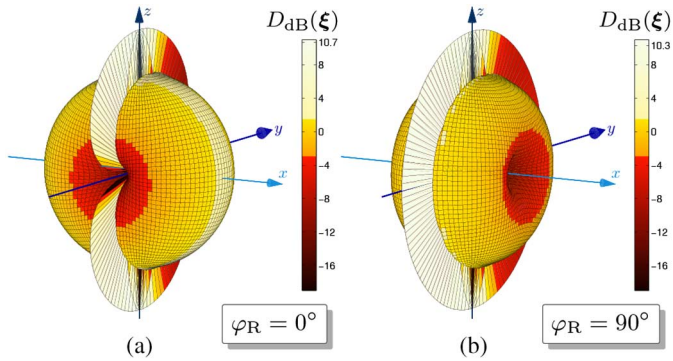

Fig. 4. $D_{dB}(\boldsymbol{\xi})$ pattern for a uniform, linear array consisting of eight rhombic antennas; $160\sqrt{2}L_R$ interelement spacing; broadside beam steering. The elements in the array are rotated at (a) $\varphi_R = 0°$ and (b) $\varphi_R = 90°$.

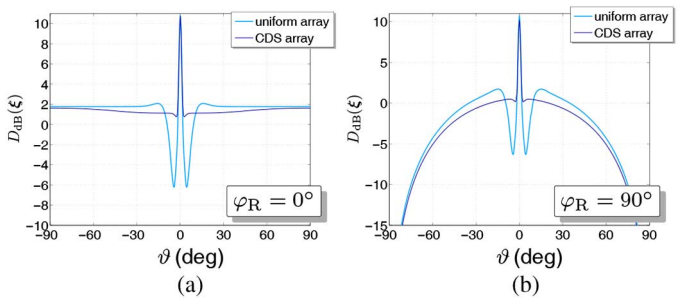

Fig. 5. Comparison between the $D_{dB}(\boldsymbol{\xi})$ for two equally long linear arrays consisting of eight rhombic antennas with uniform spacing and CDS placement, respectively; broadside beam steering. The angle ϑ assumes, conventionally, negative values in the $\varphi = 180°$ half-plane. The elements in the array are rotated at (a) $\varphi_R = 0°$ and (b) $\varphi_R = 90°$.

implicitly, total array length, thus corroborating with FD array antenna theory [1, Ch. 6]. Furthermore, despite the huge interelement spacing in Fig. 4, there is no indication of grating lobes onset. Instead, there is a single endfire sidelobe.

B. Nonuniform Array Analysis

Second, we study a nonuniform array synthesized according to the Cyclic Difference Sets (CDS) placement strategy introduced in [17]. For consistency with the analyses in Section VIII-A, the $\{57, 8, 1\}$–CDS in [18] is used,[1] thus providing eight elementary radiator positions. The initial uniform lattice employed for applying the CDS thinning is adjusted such that the array length coincides with that of a $40\sqrt{2}L_R$-spaced uniform array (four times shorter than that studied in Fig. 4).

The $D_{dB}(\boldsymbol{\xi})$ in case of the nonuniform array has the same general features as for the uniform array. For highlighting the differences, the $D_{dB}(\boldsymbol{\xi})|_{\varphi=0°\cup\varphi=180°}$ is plotted in Fig. 5 for the uniform and the CDS arrays. The two arrays provide the same beamwidth, this being a direct consequence of their lengths being the same (as is the case with FD arrays). The main difference is in the sidelobe region, where the CDS array has a more uniform behavior, with the sidelobe level being constantly below that of the uniform array, except in the region of the notches. This type of behavior can be put in correspondence with that of the FD CDS arrays that, theoretically, have a uniform sidelobe level.

[1]The plots in this section use a shifted by 12, modulo 57, cyclic permutation of the $\{57, 8, 1\}$–CDS, the largest element in the set being 38.

VIII. Conclusion

The radiation properties of array antennas composed of an arbitrary number of identical, mutually translationally shifted, pulsed electric-current excited elements were studied via a full time-domain analysis. Analytical expressions of the far-field radiated field were obtained in the case of a feeding pulse signature that can be generated by means of simple circuitry. For a unipolar pulse excitation, the radiated field distributions feature a narrow beam in conjunction with low sidelobes. Moreover, the radiation from these array antennas is free of grating lobes even for extremely wide interelement spacing. Such properties make pulsed electric-current excited arrays attractive for a range of practical applications requiring UWB operation under strict radiation mask restrictions.

Appendix

Let the straight wire segment be oriented from the point with position vector $\boldsymbol{x}_\mathcal{P}$ to the point with position vector $\boldsymbol{x}_\mathcal{Q}$, and let $\tau_{\mathcal{PQ}} = (\boldsymbol{x}_\mathcal{Q} - \boldsymbol{x}_\mathcal{P})/|\boldsymbol{x}_\mathcal{Q} - \boldsymbol{x}_\mathcal{P}|$ denote the unit vector along its tangent. Then, with $I_n(t)$ as the electric current

$$\partial_t \boldsymbol{A}_n^\infty(\boldsymbol{\xi}, t) = (\boldsymbol{x}_\mathcal{Q} - \boldsymbol{x}_\mathcal{P}) \times \int_{\lambda=0}^{1} \partial_t I_n\{t + c_0^{-1}\boldsymbol{\xi}\cdot[\lambda\boldsymbol{x}_\mathcal{Q} + (1-\lambda)\boldsymbol{x}_\mathcal{P}]\}\mathrm{d}\lambda. \quad (19)$$

1) *Case* $\boldsymbol{\xi}\cdot(\boldsymbol{x}_\mathcal{Q} - \boldsymbol{x}_\mathcal{P}) = 0$: In this case, (19) yields

$$\partial_t \boldsymbol{A}_n^\infty(\boldsymbol{\xi}, t) = (\boldsymbol{x}_\mathcal{Q} - \boldsymbol{x}_\mathcal{P})\, \partial_t I_n(t + c_0^{-1}\boldsymbol{\xi}\cdot\boldsymbol{x}_\mathcal{P}). \quad (20)$$

2) *Case* $\boldsymbol{\xi}\cdot(\boldsymbol{x}_\mathcal{Q} - \boldsymbol{x}_\mathcal{P}) \neq 0$: The use of the identity

$$\partial_t I_n(\ldots) = \frac{1}{c_0^{-1}\boldsymbol{\xi}\cdot(\boldsymbol{x}_\mathcal{Q} - \boldsymbol{x}_\mathcal{P})}\partial_\lambda I_n(\ldots) \quad (21)$$

in (19) yields in this case

$$\partial_t \boldsymbol{A}_n^\infty(\boldsymbol{\xi}, t) = (\boldsymbol{x}_\mathcal{Q} - \boldsymbol{x}_\mathcal{P})\, \frac{I_n\left(t + c_0^{-1}\boldsymbol{\xi}\cdot\boldsymbol{x}_\mathcal{Q}\right) - I_n\left(t + c_0^{-1}\boldsymbol{\xi}\cdot\boldsymbol{x}_\mathcal{P}\right)}{c_0^{-1}\boldsymbol{\xi}\cdot(\boldsymbol{x}_\mathcal{Q} - \boldsymbol{x}_\mathcal{P})}. \quad (22)$$

The results of this Appendix can serve as a building block in the designing of polyhedral wire structure arrays.

In view of (20) and (22), it is readily observed that (16) consists in this case of terms of the types

$$I_n(t+\tilde{T}_n)\; I_m(t+\tilde{T}_m) \qquad \text{for } n,m = 1,\ldots,N \quad (23)$$
$$I_n(t+\tilde{T}_n)\; \partial_t I_m(t+\tilde{T}_m) \qquad \text{for } n,m = 1,\ldots,N \quad (24)$$
$$\partial_t I_n(t+\tilde{T}_n)\; \partial_t I_m(t+\tilde{T}_m) \qquad \text{for } n,m = 1,\ldots,N \quad (25)$$

with $\tilde{T}_n$ and $\tilde{T}_m$ representing the "time delays" occurring in the relevant expressions. These terms need being multiplied by geometry-dependent factors $(\boldsymbol{x}_\mathcal{Q} - \boldsymbol{x}_\mathcal{P})_n \cdot (\boldsymbol{x}_\mathcal{Q} - \boldsymbol{x}_\mathcal{P})_m$ and, possibly, divided by $c_0^{-1}\boldsymbol{\xi}\cdot(\boldsymbol{x}_\mathcal{Q} - \boldsymbol{x}_\mathcal{P})$, when applicable.

For the excitation in (18), these terms require the evaluation of integrals of the type

$$\int_{u=0}^{\infty} u^p \exp(-qu)\mathrm{d}u = \mathcal{L}\left(u^p\right)|_{s=q} = \frac{p!}{q^{p+1}} \quad \text{with } p>0 \text{ and } q>0, p, q \in \mathbb{N} \quad (26)$$

where $\mathcal{L}(\cdot)$ indicates the Laplace transform. Since (18) uses the normalized time coordinate $t' = t/t_\mathrm{r}$ and by taking $\Delta_t' = [\max(\tilde{T}_n, \tilde{T}_m) - \min(\tilde{T}_n, \tilde{T}_m)]/t_\mathrm{r}$, (23)–(25) yield

$$\mathcal{I} = \mathcal{K} t_\mathrm{r} \sum_{k=0}^{\nu}\left[\frac{\nu!\Delta_{t'}^k}{(\nu-k)!k!}\frac{(2\nu-k)!}{(2\nu)^{2\nu-k+1}}\right] \quad (27)$$

$$\mathcal{I}_\partial = \mathcal{K}\nu \sum_{k=0}^{\nu}\left[\frac{\nu!\Delta_{t'}^k}{(\nu-k)!k!}\frac{(2\nu-k-1)!}{(2\nu)^{2\nu-k+1}}\mathrm{sign}(t_n - t_m)k\right] \quad (28)$$

$$\mathcal{I}_{\partial\partial} = \mathcal{K}\frac{\nu^2}{t_\mathrm{r}} \sum_{k=0}^{\nu}\left[\frac{\nu!\Delta_{t'}^k}{(\nu-k)!k!}\frac{(2\nu-k-2)!}{(2\nu)^{2\nu-k+1}}(2\nu - k^2 - k)\right] \quad (29)$$

with $\mathcal{I}$, $\mathcal{I}_\partial$, and $\mathcal{I}_{\partial\partial}$ denoting the integrals $\int_{t=0}^{\infty}(\cdot)\mathrm{d}t$ of the expressions in (23)–(25), respectively, $\mathrm{sign}(x) = \{-1, 0, 1\}$ for $\{x<0, x=0, x>0\}$, and $\mathcal{K} = \exp[\nu(2-\Delta_t')]$.

References

[1] C. A. Balanis, *Antenna Theory: Analysis and Design*, 2nd ed. New York, NY, USA: Wiley, 1997.

[2] S. Ries and T. Kaiser, "Ultra wideband impulse beamforming: It is a different world," *Signal Process.*, vol. 86, pp. 2198–2207, Feb. 2006.

[3] A. Shlivinski, E. Heyman, and R. Kastner, "Antenna characterization in the time domain," *IEEE Trans. Antennas Propag.*, vol. 45, no. 7, pp. 1140–1149, Jul. 1997.

[4] A. Shlivinski and E. Heyman, "A unified kinematic theory of transient arrays," in *Ultra-Wideband, Short-Pulse Electromagnetics*, P. D. Smith and S. R. Cloude, Eds. New York, NY, USA: Kluwer/Plenum, 2002, vol. 5, pp. 327–334.

[5] G. Marrocco and M. Ciattaglia, "Ultrawide-band modeling of transient radiation from aperture antennas," *IEEE Trans. Antennas Propag.*, vol. 52, no. 9, pp. 2341–2347, Sep. 2004.

[6] G. Franceschetti, J. Tatoian, and G. Gibbs, "Timed arrays in a nutshell," *IEEE Trans. Antennas Propag.*, vol. 53, no. 12, pp. 4073–4082, Dec. 2005.

[7] M. Ciattaglia and G. Marrocco, "Time domain synthesis of pulsed arrays," *IEEE Trans. Antennas Propag.*, vol. 56, no. 7, pp. 1928–1938, Jul. 2008.

[8] G. Marrocco and M. Ciattaglia, "Hermite-rodriguez UWB circular arrays," *IEEE Trans. Antennas Propag.*, vol. 58, no. 2, pp. 381–390, Feb. 2010.

[9] J. S. McLean, H. Foltz, and R. Sutton, "Pattern descriptors for UWB antennas," *IEEE Trans. Antennas Propag.*, vol. 53, no. 1, pp. 553–559, Jan. 2005.

[10] A. Shlivinski, "Kinematic properties of short-pulsed sparse transmitting arrays," *Prog. Electromagn. Res.*, vol. 115, pp. 11–33, 2011.

[11] E. Pancera, T. Zwick, and W. Wiesbeck, "Spherical fidelity patterns of UWB antennas," *IEEE Trans. Antennas Propag.*, vol. 59, no. 6, pp. 2111–2119, Jun. 2011.

[12] J. C. Bogerd, A. G. Tijhuis, and J. J. A. Klaasen, "Electromagnetic excitation of a thin wire: A traveling-wave approach," *IEEE Trans. Antennas Propag.*, vol. 46, no. 8, pp. 1202–1211, Aug. 1998.

[13] A. T. de Hoop, "Electronic version (with corrections) 2008, freely downloadable, for private use," in *Handbook of Radiation and Scattering of Waves*. London, U.K.: Academic, 1995.

[14] I. E. Lager and A. T. de Hoop, "Loop-to-loop pulsed electromagnetic field wireless signal transfer," in *Proc. 6th EuCAP*, Prague, Czech Republic, Mar. 2012, pp. 786–790.

[15] I. E. Lager, A. T. de Hoop, and T. Kikkawa, "Model pulses for performance prediction of digital microelectronic systems," *IEEE Trans. Compon., Packag., Manuf. Technol.*, vol. 2, no. 11, pp. 1859–1870, Nov. 2012.

[16] J. G. Chaney, "Free space radiation impedance of rhombic antenna," *J. Appl. Phys.*, vol. 24, no. 5, pp. 536–540, May 1953.

[17] D. G. Leeper, "Isophoric arrays–massively thinned phased arrays with well-controlled sidelobes," *IEEE Trans. Antennas Propag.*, vol. 47, no. 12, pp. 1825–1835, Dec. 1999.

[18] D. Gordon, "La Jolla cyclic difference set repository," [Online]. Available: http://www.ccrwest.org/diffsets.html